Low-temperature O_2^- mobility in high-density neon gas

A. F. Borghesani, D. Neri, and M. Santini
Dipartimento di Fisica "G. Galilei," Università di Padova and Consorzio Interuniversitario Fisica della Materia, Via F. Marzolo 8, I-35131 Padova, Italy
(Received 26 February 1993)

We report measurements of the drift mobility of O_2^- ions in supercritical neon gas at high density at a temperature $T = 45.03$ K, 0.6 K above the critical temperature. Our measurements span a very large density range, up to values comparable with those of a liquid [$(15–240)\times10^{20}$ cm^{-3}], and cover the transition region from the kinetic to the hydrodynamic regime. We show that the classical hydrodynamic Stokes formula for the drag on a sphere moving through a fluid describes accurately enough the ionic mobility as a function of the gas density, if it is modified to take into account the spatial dependence of the gas density and viscosity around the ion due to electrostriction.

PACS number(s): 51.50.+v, 52.25.Fi

I. INTRODUCTION

Understanding the motion of ions in gases under the influence of an electric field is of great importance in many areas of physics. In low-density gases the ionic mobility is primarily determined by the cross section for momentum transfer. Within the frame of the Boltzmann formalism, information on the ion–neutral-species interaction potential can be gathered from mobility data [1–3].

On the other side, thermal ions were successfully used as a probe to investigate the microscopic behavior and structure of dense fluids, such as superfluid helium [4–17], cryogenic liquids [18–20], and liquid hydrocarbons [21,22], within the frame of reference of continuum mechanics.

The intermediate region between the low-density gas and the high-density liquid is important to the purpose of studying the transition from the kinetic regime to the hydrodynamic one. In spite of the relevance of this subject there are few systematic studies to be found in the literature [21,23,24]. The reason might be that there are both experimental difficulties as well as theoretical ones due to the lack of a well assessed theory.

The typical experiments in this field are carried out by observing the drift mobility of ions generated by ionizing the gas with a short x-ray pulse [23]. From a technical point of view, this technique of ion generation adds to the complexity of the experimental setup. On the other hand, from a conceptual point of view, this technique restricts the research field to ions in their parent gases, Ar^+ in Ar, for instance. This fact has the drawback that the probe used, the ion, is different as the gas under study is changed.

An ion common to all gases, however, can be easily generated in experiments based on the pulsed photoemission technique by exploiting the process of resonant attachment of electrons to O_2 molecules, yielding O_2^- [25–29]. O_2 impurities are practically found in every gas. For instance, in the best commercially available neon gas, the amount of O_2 is approximately 50 ppm. This amount is huge if the electron mobility is to be measured in high-density gases, where an O_2 impurity concentration in the tenths of ppb range is required in order to have free electrons drifting through the whole space between the electrodes. But it is large enough to produce a detectable amount of ions, whose drift motion can be easily observed with suitable electronics.

Advantages and drawbacks of this technique are immediately evident: (i) the same ionic species is used throughout, so that specific features of the particular gas under study can be brought into evidence; (ii) different types of negative ions can be studied by suitably reducing the O_2 impurity concentration down to some tenths of ppb when no detectable signal from O_2^- is observed [27], and introducing in the chamber a suitable concentration (some tens of ppm) of an electron-attaching gas; (iii) the very simple and reliable pulsed photoemission technique can be used; (iv) the ionic concentration is low enough to neglect ion-ion interaction; (v) at too small gas densities the number of ions produced is small and they cannot be easily detected.

O_2^- mobility measurements in high-density He gas at 77.6 K were already carried out in the past, though in an unsystematic way [30]. These measurements brought into evidence two unexpected facts: (i) a systematic increase with the gas density of the reduced mobility at zero electric field; (ii) a strong disagreement of the reduced mobility value extrapolated down at zero density with the prediction of the Langevin theory [31,32]. This disagreement could not be overcome even by assuming the presence of heavier, clustered negative ions, such as O_4^- [30].
These two points remained unexplained because of the lack of a suitable theory and, maybe, for the lack of a real interest in this subject [33].

In the past few years, in our laboratory, we have constructed and used an apparatus based on the pulsed photoemission technique in order to study the electronic mobility and resonant attachment to O_2 in high-density neon gas [34–36,27]. In the cell of our apparatus, at

fairly low temperatures, a neon gas density twice as large as the density of the liquid at the critical point can be easily attained. Owing to this opportunity, we have decided to carry out systematic measurements of O_2^- mobility in high-density neon gas. In this paper we report the results obtained at T =45.03 K in the density range $(15 \leq N \leq 235) \times 10^{20}\,\mathrm{cm}^{-3}$.

II. EXPERIMENTAL DETAILS

We have used the same pulsed photoemission technique and apparatus exploited for the measurements of electron drift mobility in high-density neon gas. The apparatus has been thoroughly described elsewhere [34–38]. We recall here only its most important features.

A. General details

Two parallel-plate circular electrodes are contained inside a brass cell that can withstand pressure up to 15 MPa. The cell is mounted on the cold head of a cryocooler (CTI, model 21) inside a homemade cryostat. The two electrodes are made of gold-plated brass, and are separated by a distance $d \approx 0.4$ cm. Their radius is $R_e \approx 3$ cm, so that their aspect ratio $R_e/d \approx 7.5$ is large enough to comply with the requirement of ideal geometry $[(R_e/d)_{\min} \approx 2.5]$ [37]. In this situation the integration of the current induced by a bunch of ions moving through the drift space yields a linear voltage wave form.

The anode is connected to a passive RC network in order to integrate the ionic current. Integration of the current is necessary in order to improve the signal-to-noise ratio in our experimental conditions [39]. The time constant of the circuit is $RC \approx 5$ s. Such a large value is required because the ionic transit time in our experimental conditions can be as large as 1 s.

The second electrode acts as a photocathode. Production of photoelectrons is accomplished by irradiating it with a 4 μs short UV pulse of a Xe flashlamp (EG&G, model FX108AU). Approximately 2×10^4 to 2×10^6 electrons per pulse are extracted and injected into the drift space, depending on the gas density. The electrons attach readily to O_2 impurities generating slow O_2^- ions drifting toward the anode under the influence of the applied electric field.

The amount of O_2 molecular impurities is fairly low. The neon gas used has a nominal impurity content of 50 ppm. To remove impurities like water vapor, carbon dioxide, residual hydrocarbons, and part of O_2, the gas is passed through an activated charcoal trap immersed in liquid nitrogen. An upper limit to the residual O_2 content can be estimated as follows. Since the O_2 triple point is much higher than our working temperature ($T \approx 45$ K), O_2 solidifies when its partial pressure equals the sublimation pressure at that temperature [40] and the photocathode efficiency should decrease because of solid O_2 deposition. This fact was observed during electron-mobility measurements in neon gas carried out with the same apparatus. As we did not detect any loss of photocathode efficiency even at the largest neon gas pressures during the present experiment, we conclude that the O_2 partial pressure was lower than that corresponding to an O_2 impurity concentration of 10 ppm.

Since the number of electrons injected, and hence the number of O_2^- ions produced, is small, the electrical signals are also fairly small and electrical noise must be carefully minimized. The major source of noise is due to mechanical vibrations of the electrode assembly induced by the reciprocating displacer of the cryocooler head. Especially at large applied fields the ionic signal might be completely obscured by noise. Therefore, the cell and the amplifier were mechanically decoupled from the cryocooler head by means of four copper cantilevers. By so doing, a very good noise reduction was achieved, while keeping a satisfactory thermal contact with the cryocooler head [36].

B. Signal wave form analysis

The current induced by the drifting charges is integrated by means of a passive RC network. The integrator output is linearly amplified by a factor 100 and is recorded by a digital storage oscilloscope (Hitachi, model VC 6041). The digitized wave form is then sent to a personal computer (Apple Macintosh IICi) over a general-purpose interface bus (GPIB) and numerically analyzed. The analysis of the signal wave form allows the determination of the drift parameters, first of all the ionic drift time.

Provided that the electronic transit time τ_e is much smaller than the ionic one τ_i as usual, it is easy to show that the ionic wave form is given by [39]

$$v_i(t) = -v_T \left(I - P(A,I)e^{-t/RC} - Q(A,I)e^{-At/\tau_i} \right) \quad \text{for } 0 \leq t \leq \tau_i. \quad (1)$$

In Eq. (1) $v_T = (en_0)/C$ is the maximum attainable signal amplitude, (en_0) is the total charge photoinjected into the drift space, and C is the total integrating capacitance (in our case $C \approx 40$ pF). $I = (RC)/\tau_i$ is the ratio of the integrator time constant to the ionic drift time, $A = \nu_A \tau_e$ is the attachment efficiency, and ν_A is the electron attachment rate. P and Q are functions of A and I and are given by

$$P = \frac{e^{-A} + (AI)^2 - 1}{A(AI+1)} \quad (2)$$

and

$$Q = \frac{Ie^{-A}}{(AI+1)} \quad (3)$$

For $t \geq \tau_i$ the signal shows the usual exponential decay

$$v_i(t) = v_i(\tau_i)e^{-(t-\tau_i)/RC}. \quad (4)$$

The signal wave form may look very different according to the values of the parameters A and I. In the present

experiment, for neon gas densities $N \geq 50 \times 10^{20}$ cm^{-3}, the attachment rate ν_A is fairly large and $A \gg 1$. In this case the ions are generated in close proximity of the cathode. Since $I > 1$, as usual, also $AI \gg 1$ and Eq. (1) reduces to

$$v_i(t) = -v_T \left(\frac{t}{\tau_i}\right) \qquad \text{for } 0 \leq t \leq \tau_i \tag{5}$$

and Eq. (4) becomes

$$v_i(t) = -v_T e^{-(t-\tau_i)/RC} \quad \text{for } t > \tau_i. \tag{6}$$

In this situation the transit time of the ion swarm can be accurately determined from an extrapolation of the linearly changing voltage wave form to find the start and end points of the ionic motion in the drift space. A typical experimentally recorded signal is shown in Fig. 1.

For lower densities, condition $A \gg 1$ may not be satisfied and the drift parameters must be determined by the analysis of the wave form given by Eq. (1). A typical signal recorded in these conditions is shown in Fig. 2.

In principle, standard nonlinear least-squares-fit techniques could be used to determine the three parameters A, I, and v_T. In practice, since each wave form consists of 4000 points and since several hundreds of wave forms are collected during each experimental run, this solution is unsuitable because it is much too time consuming. Therefore, we have adopted a different method, similar to that known as "three-points method" devised for the analysis of the electronic wave form and described elsewhere [39]. Summarizing, three points $\{[(t_j, v_j \equiv v_i(t_j)], j = 1,2,3\}$ are chosen from the signal and the parameters A, I, and v_T are adjusted so as to fit the analytical wave form to them.

Letting $B = (v_1/v_3)$ be the ratio of the voltage values of the experimental signal, we define the functions

$$G = I(1-B) - (e^{-t_1/RC} - Be^{-t_3/RC}) \times [P(A,I) + Q(A,I)] \tag{7}$$

and

$$D = (v_2)_c - v_2 \tag{8}$$

where $(v_2)_c$ is the value of $v_i(t)$ calculated for $t = t_2$

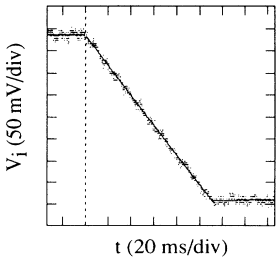

FIG. 1. Ionic signal wave form at high density when the attachment rate is fairly large, $A \gg 1$. No electronic contribution is present. Experimental parameters: $E = 583$ V/cm, $\tau_i = 111.0$ ms, $N = 231.9 \times 10^{20}$ cm^{-3}.

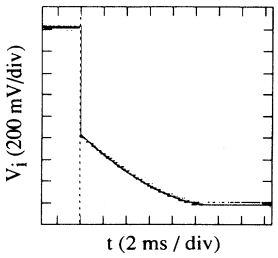

FIG. 2. Signal wave form at smaller density when the attachment rate is not very large, i.e., $A \simeq 1$. The signal jump at $t = 0$ is the contribution due to the fast electrons. The following slow part of the signal is due to the ions. The analytical wave form calculated according to Eq. (1) with parameters determined with the three-points method described in the text is also shown. Experimental parameters: $E = 1554$ V/cm, $\tau_i = 11.60$ ms, $N = 39.36 \times 10^{20}$ cm^{-3}.

according to Eq. (1), with the auxiliary equation

$$v_T = -\frac{v_1}{I - Pe^{-t_1/RC} - Qe^{-At_1/\tau_i}}. \tag{9}$$

If the true values of A, I, and v_T were known, then both $G = 0$ and $D = 0$. So, we are facing a double root-finding problem which can be solved iteratively using standard algorithms [41]. Only an initial value for τ_i has to be guessed in order to start the iteration, since the initial value of A is determined by the relation

$$A = \tau_i \left(\frac{1}{RC} + \frac{v'_i(0)}{v_i(0)}\right) \tag{10}$$

where

$$v'_i(0) = \left(\frac{dv_i(t)}{dt}\right)_{t=0} \tag{11}$$

as easily derived from Eq. (1). Iteration is stopped when both G and D are simultaneously zeroed within a given accuracy. Normally, the convergence criterion is $|D| \leq 2 \times 10^{-4} v_2$. At the end of the iteration τ_i is calculated from the relation $\tau_i = RC/I$. The agreement between the experimental signal and the one calculated according to Eq. (1) with the parameters A, I, and v_T determined with this iterative procedure is very good, as shown in Fig. 2.

C. Experimental accuracy

The ionic mobility is determined from the measured transit time as

$$\mu = \frac{d^2}{\tau_i V} \tag{12}$$

where d is the drift distance and V is the potential difference between the electrodes. The relative accuracy of the mobility determination can be then calculated according to the usual error propagation formulas.

The drift distance $d = 0.386$ cm is known with an

accuracy $|\Delta d/d| \approx 2\%$. $|\Delta V/V|$ is negligible since the dc cell resistance ($R_c \approx 10^{18}\ \Omega$) is much larger than the amplifier input resistance ($R \approx 10^{11}\ \Omega$).

The determination of the accuracy of the drift time measurements is more difficult. When the ionic signal is a straight line, it can be shown [42] that

$$\left|\frac{\Delta\tau_i}{\tau_i}\right| \approx \frac{3}{S} \tag{13}$$

where S is the signal-to-noise ratio. In our experimental conditions $S \geq 100$. So, we get $|\Delta\tau_i/\tau_i| \leq 3\%$. If the ionic signal has to be analyzed by means of the three-points method, there is no simple way to determine $|\Delta\tau_i/\tau_i|$. One empirical way to estimate it is to repeatedly analyze the same signal by choosing at random the three points. By so doing, we obtained a dispersion around the mean value of approximately 2%.

Since the three-ponts method is very sensitive to the signal shape, the presence of electrical noise might influence the parameter determination. This effect is difficult to predict but it can be estimated to influence to less than 5% the drift time measurements under the signal-to-noise ratio values of our experiment. Thus, the overall accuracy of our measurements can be estimated to be $|\Delta\mu/\mu| \leq 7\%$.

One more interesting quantity in our measurements is the so called density-normalized mobility, μN, where N is the gas density. This is calculated from the experimental temperature and pressure data according to the state equation of McCarty and Stewart [43]. Pressure is read by means of a digital gauge (Ashcroft, model Digigauge 7780) with an accuracy $|\Delta P/P| \leq 0.5\%$ and temperature is measured using an ac ratio-transformer bridge and a Pt sensor. The cell temperature is stabilized within 0.01 K. Thus, the accuracy of the density determination at 45 K turns out to be $|\Delta N/N| \leq 1\%$.

III. EXPERIMENTAL RESULTS AND DISCUSSION

In Fig. 3 we show the measured O_2^- mobility at $T = 45$ K as a function of the density-reduced electric-field (E/N) for some of the investigated neon gas densities. For all of the densities but the lowest one the ionic mobility is field independent over more than one order of magnitude in (E/N). This means that the mean ion energy is essentially thermal and that the measurements are carried out in the low electric-field limit. The weak electric-field dependence of the mobility at the lowest density is probably an instrumental effect due to the difficulty of analyzing the signal wave form when the ionic contribution to it is too small, i.e., when $A \leq 1$.

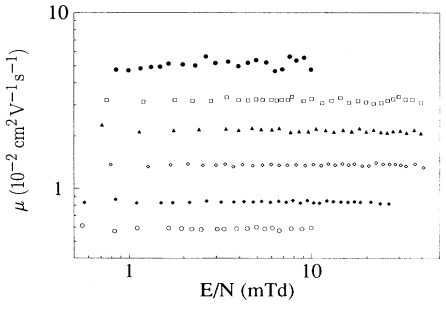

FIG. 3. Ionic mobility as a function of the density-reduced electric field E/N(1 Td = 10^{-17} V cm^{-2}) for some of the investigated gas densities at $T = 45.03$ K. The densities are (from top to bottom) $N = (15.69, 26.30, 39.36, 63.54, 98.77, 234.5) \times 10^{20}$ cm^{-3}.

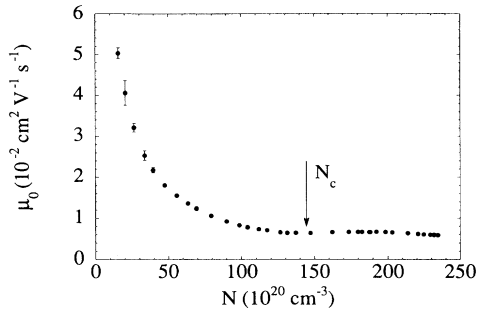

FIG. 4. Experimental zero-field mobility μ_0 as a function of the gas density. $N_c = 144.3 \times 10^{20}$ cm^{-3} is the critical density of neon.

In Fig. 4 we report the mobility values extrapolated to zero electric field μ_0 as a function of the gas density N. In Fig. 5 we show the zero-field density-normalized mobility $\mu_0 N$ as a function of N. The behavior of $\mu_0 N$ is rather complex, but is very similar to that of the mobility of cations Ar^+, N_2^+, and CH_4^+ in their parent gases [23]. We can distinguish three density regions. There is a first region, from $N = 0$ up to approximately $N = (120\text{–}130) \times 10^{20}$ cm^{-3}, where $\mu_0 N$ is nearly constant. In the second region, for $(130 < N < 200) \times 10^{20}$ cm^{-3}, $\mu_0 N$ increases linearly with N. Finally, for $N > 200 \times 10^{20}$ cm^{-3} $\mu_0 N$ saturates to a constant value again.

In the first density region $\mu_0 N$ is nearly independent of the gas density, as would be predicted by the classical kinetic theory if binary scattering controls ion transport [31]. $\mu_0 N$ can be extrapolated down to zero density

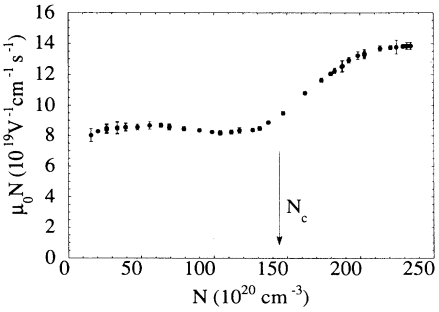

FIG. 5. Experimental zero-field density-normalized mobility $\mu_0 N$ as a function of the gas density. The critical density of neon, N_c, is indicated by an arrow.

with fairly good confidence because of its weak density dependence, and also because measurements carried out at room temperature at densities as low as $N \simeq 0.2 \times 10^{20}\,\mathrm{cm}^{-3}$ did not show any "strange" behavior of the mobility at small density [42]. We obtain

$$(\mu_0 N)_0 = (8.2 \pm 0.4) \times 10^{19}\ (\mathrm{V\ cm\ s})^{-1} \tag{14}$$

which should correspond to the density-normalized mobility value predicted by the kinetic theory. In fact, if binary scattering controls ion transport, the solution of the Boltzmann equation yields a constant $\mu_0 N$, independent of N. Moreover, since the ions are in thermal equilibrium with the atoms of the host gas, their thermal energy is quite low ($k_B T \approx 3.9 \times 10^{-3}$ eV at $T = 45$ K). This means that the scattering is governed by the polarization potential due to the interaction of the ionic charge and the dipole moment induced by it on the neon atom. Therefore, in this low-density limit $\mu_0 N$ should approach the so-called *polarization limit* given by [23]

$$(\mu_{\mathrm{pol}} N) = \frac{4.81 \times 10^{-4}}{(\alpha M_r)^{1/2}} \tag{15}$$

where α is the atomic polarizability of neon, expressed in units of cm^3, and M_r is the O_2-Ne reduced mass, in g/molecule. For Ne $\alpha = 0.3946 \times 10^{-24}$ cm^3 and $M_r = 2.055 \times 10^{-23}$ g [44] and we obtain

$$(\mu_{\mathrm{pol}} N) \simeq 16.89 \times 10^{19}\ (\mathrm{V\ cm\ s})^{-1}.$$

So, at low density, even if $\mu_0 N$ is quite independent of N, as predicted by the kinetic theory, nonetheless its value is smaller than the predicted one by nearly a factor 2. Such a discrepancy has been also found in many other systems [23,30]. It has been argued that ions could be clustered [23]. In this case, M_r in Eq. (15) should be taken to be approximately equal to the atomic mass of neon and we would obtain

$$(\mu_{\mathrm{pol}} N)_{\mathrm{CI}} \simeq 13.23 \times 10^{19}\ (\mathrm{V\ cm\ s})^{-1}$$

where CI means *clustered ions*. This value is again much greater than experimentally observed. The problem is that classical kinetic theory can be used if the ionic mean free path is much larger than the atomic diameter in order that the O_2^- ion undergoes collisions only with one atom at a time. A rough estimate of the ion mean free path, ℓ, can be obtained using the Drude result for the mobility [45]

$$\ell \approx \frac{M_r \bar{v}_r \mu}{e} \tag{16}$$

where M_r is the reduced mass of the O_2 - Ne system and $\bar{v}_r$ is a mean relative velocity, for instance,

$$\bar{v}_r = \left(\frac{3 k_{\mathrm{B}} T}{M_r}\right)^{1/2}. \tag{17}$$

Here k_{B} is the Boltzmann constant. For $N = 15.7 \times 10^{20}\,\mathrm{cm}^{-3}$ and $T = 45$ K we measured $\mu = 5.13 \times 10^{-2}$ $\mathrm{cm}^2/\mathrm{V\,s}$ and we obtain $\ell \simeq 2$ Å. If the ion were completely clustered, we would obtain $\ell \simeq 2.5$ Å. These mean free path values are to be compared with the Lennard-Jones diameter of neon $\sigma_{\mathrm{LJ}} = 2.76$ Å [44] or with the O_2^--Ne hard-sphere diameter which can estimated to be $\sigma_{O_2^-} = 3.2$ Å [42,44], and with the average interatomic spacing $\bar{d} \simeq (N)^{-1/3} = 8.6$ Å. It is evident that in our experiment, even at the lowest densities, the conditions for the use of classical kinetic theory are not fulfilled. Also the Enskog theory for transport phenomena in dense gases, which takes into account the finite size of molecules, is in disagreement with our measurements, since it predicts a monotonic, though small, decrease of the density-normalized mobility with increasing gas density [46].

In the high-density region the gas density is comparable to that of the liquid (we recall that the critical density of neon is $N_c = 144.3 \times 10^{20}\,\mathrm{cm}^{-3}$ and its critical temperature is $T_c = 44.38$ K [43]), and it is assumed that hydrodynamics can be used to describe the ionic motion. The hydrodynamic picture is based on the assumption that the mean free path of the atoms of the liquid is smaller than the dimensions of the foreign object moving through it. If we treat the neon atoms as hard spheres of diameter σ_{LJ}, the Ne-Ne cross section can be estimated as

$$Q_{\text{Ne-Ne}} = \pi(\sigma_{\mathrm{LJ}})^2 \simeq 24\ \text{Å}^2 \tag{18}$$

which is consistent with the neon cross section deduced from viscosity data [31], and then the mean free path becomes

$$\ell_{\mathrm{Ne}} = \frac{1}{N Q_{\text{Ne-Ne}}} = 1.7\,\text{Å} \qquad \text{for } N = 240 \times 10^{20}\,\mathrm{cm}^{-3} \tag{19}$$

to be compared with an average interatomic spacing $\bar{d} \simeq 3.5$ Å. Moreover, molecular dynamics calculations [47] have shown that the strong attractive force exerted by the ion on the polarizable particles of the fluid leads to the formation of a tightly packed solvation shell around the ion. Assuming that this shell consists of one complete layer of neon atoms clustered around the ion, the outer radius R of this complex can be estimated to be

$$R \simeq \tfrac{1}{2}(\sigma_{O_2^-} + \sigma_{\mathrm{LJ}}) = 4.36\,\text{Å}. \tag{20}$$

It therefore appears that the use of hydrodynamics at the highest densities of our experiment is correct, while it seems not justified at the low densities, where the mean free path of the neon atoms is much larger (for instance, $\ell_{\mathrm{Ne}} \simeq 27$ Å for $N = 15.6 \times 10^{20}\,\mathrm{cm}^{-3}$).

The hydrodynamic formula for the mobility of a sphere of radius R is the well-known Stokes formula [48]

$$\mu = \frac{e}{6\pi\eta R} \tag{21}$$

where η is the fluid viscosity and the constant 6π arises from the so-called "stick" boundary conditions which apply in the case of an ion. It is well known [49] that Stokes's law makes nearly correct quantitative predictions even in the case of microscopic objects, which are not large compared to the fluid atoms nor are they much

more massive. Henceforth, we will assume Stokes's law as granted.

Stokes's formula applies if the nonlinear terms in the Navier-Stokes equation can be dropped, i.e., for small Reynolds numbers, $\mathcal{R} \ll 1$. In our case $\mathcal{R}$ can be calculated according to the following formula:

$$\mathcal{R} = \frac{\rho \mu E R}{\eta} \tag{22}$$

where ρ and η are the mass density and viscosity of neon, μ is the ion mobility, E is the applied electric field, and R is the ion (or cluster) radius. In the worst case during our experiment $\mathcal{R} \simeq 3 \times 10^{-2} << 1$. So, the conditions for the applicability of the Stokes law are satisfied.

In Fig. 6 we show $\mu\eta$ as a function of N. η at $T = 45$ K has been interpolated from experimental data reported in the literature [50]. From Stokes's law, Eq. (21), the product $\mu\eta$ should be a constant for a constant hydrodynamic radius R at high density. On the contrary, $\mu\eta$ at low density should be inversely proportional to N, since in the kinetic regime the viscosity is related to the neon mean free path according to the formula [51]

$$\eta = \tfrac{1}{3} N M_{\mathrm{Ne}} \bar{v}_{\mathrm{Ne}} \ell_{\mathrm{Ne}} \tag{23}$$

and does not depend on N.

From this figure it is clear that (i) at the lowest density the kinetic regime has not been completely attained yet; and (ii) in the high-density region the assumption of a constant hydrodynamic radius is incompatible with the experimental results. Nonetheless, the validity of the Stokes formula could be preserved by assuming that the hydrodynamic radius of the ion depends on the density. Thus, the mobility data can be used to calculate this density-dependent radius. In order to take into account the fact that our data cover the transition region from the kinetic to the hydrodynamic region, we need an interpolation formula connecting the ideal gas and ideal liquid limits of ion transport. The first attempt is due to Cunningham [52,53], who modified the Stokes law into the following formula:

$$\mu = \frac{e}{6\pi\eta R}\left(1 + A\frac{\ell}{R}\right) \tag{24}$$

where A is a constant and ℓ is the mean free path between collisions. In normal liquids $\ell \ll R/A$, and Stokes's law is recovered. Equation (24) has been modified so as to successfully treat the transport of localized electrons in liquid helium [54], in high-density neon gas [36], and in some liquid hydrocarbons [55]. The constant A was taken as $\frac{3}{2}$ and the kinetic expression for ℓ was used:

$$\ell = \frac{3\eta}{M_r \bar{v}_r N}. \tag{25}$$

By substituting this expression into Eq. (24) we get

$$\mu = \frac{e}{6\pi\eta R}\left(1 + \frac{9\pi\eta}{4NR(2\pi M_r k_{\mathrm{B}} T)^{1/2}}\right). \tag{26}$$

At low density, where $\ell \gg R$, Eq. (26) becomes

$$\mu = \frac{3e}{8N}\left(\frac{\pi}{2M_r k_{\mathrm{B}} T}\right)^{1/2} \frac{1}{\pi R^2} \tag{27}$$

which is the rigorous result of the kinetic theory for the mobility of hard spheres of radius R and cross sections $Q_{\mathrm{HS}} = \pi R^2$. However, in Eqs. (25) and (26) we have used $M_r = M_{\mathrm{Ne}}$, since we have seen that ions are very likely to be clustered.

In Fig. 7 we plot the correction term $3\ell/2R$ as a function of N, computed by using Eq. (25) for ℓ, and assuming $R = (1/2)(2\sigma_{\mathrm{LJ}} + \sigma_{O_2}) = 4.36$ Å, which corresponds to the hard-sphere radius of an O_2^- ion surrounded by one complete solvation shell of Ne atoms. It can be noted that this correction term increases with density at high densities and this corresponds to an unrealistic increase with density of the mean free path as computed by means of a formula, Eq. (25), that holds true only in the kinetic regime [51]. It seems therefore more plausible to compute the mean free path ℓ according to the classical relation

$$\ell = \frac{1}{NQ} \tag{28}$$

where Q is the total cross section. We have used here

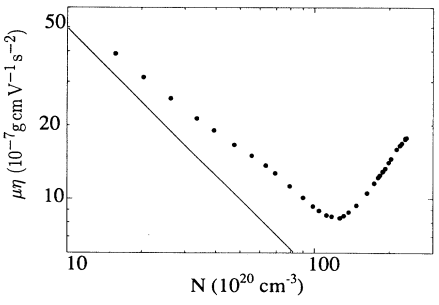

FIG. 6. The viscosity-mobility product $\mu\eta$ as a function of the gas density. At low density $\mu\eta$ should possess the slope of the straight line shown if the kinetic regime were obeyed. At high density, $\mu\eta$ should be constant if the hydrodynamic radius of the ion were constant.

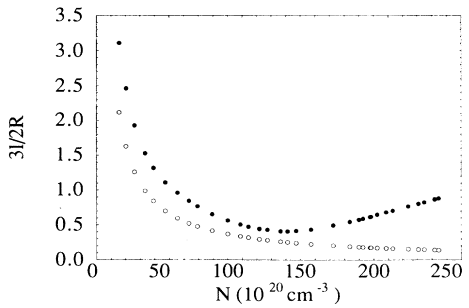

FIG. 7. Kinetic correction $3\ell/2R$ in the Stokes-Cunningham formula as a function of the gas density. Closed points: Eq. (25); open points: Eq. (28).

the hard-sphere kinetic cross section $Q = \pi\sigma^2 \simeq 110$ Å^2, where $\sigma = (\sigma_{LJ} + \sigma_{O_2})/2 + \sigma_{LJ} \simeq 5.74$ Å pertains to the binary collision of a clustered ion with a Ne atom. Equation (28) is again a kinetic expression (that gives the correct expression for μ at low density), but it does not predict any increase of ℓ/R with N at high density, as shown in Fig. 7.

By inserting Eq. (28) into Eq. (24) we get

$$\mu = \frac{e}{6\pi\eta R}\left(1 + \frac{3}{2NQR}\right). \tag{29}$$

We can now use the experimental mobility data to compute the (semi)hydrodynamical radius R of the ion. In Fig. 8 we report R computed according to Eqs. (21), (26), and (29) as a function of the gas density N. All the three curves show a similar density dependence. The computed radius increases rapidly with N at low to medium density. It shows a maximum close to $N = 130 \times 10^{20}$ cm^{-3}, and then decreases with increasing N, approximately saturating to a constant value for large N.

At very high density, where a "pure" hydrodynamic regime is to be expected, Stokes's formula Eq. (21) gives a radius R close to the value 4.36 Å corresponding to a complete tightly packed solvation shell of neon atoms around the ion. Also Eq. (29) gives a radius close to 4.36 Å, as is to be expected since the correction term $3/(2NQR)$ is quite small. On the other hand, Eq. (26) fails to predict a reasonable value for R at large density because of the unrealistic behavior of the correction term computed with the aid of Eq. (25).

From Fig. 8 we can also note immediately the inadequacy of the pure hydrodynamic Stokes formula at low density, where it predicts a radius close to zero at zero density, as well as the inadequacy of the semihydrodynamic formula Eq. (26), which predicts an inconsistently large radius at low density. On the contrary, the semihydrodynamic formula Eq. (29) predicts a low-density radius self-consistently close to the value $\sigma = 5.74$ Å used to compute the hard-sphere cross section for the collision of the clustered ion off a neon atom. It seems therefore that the semihydrodynamic formula Eq. (29) can be safely used as an interpolation between the kinetic and hydrodynamic regimes.

In any case, whatever formula is used [Eqs. (21), (26), or (29)], the computed semihydrodynamic radius shows the general feature of a maximum at a density close to, but smaller than, the critical one. In order to explain these observations, at least semiquantitatively, we refer to the electrostriction model originally developed

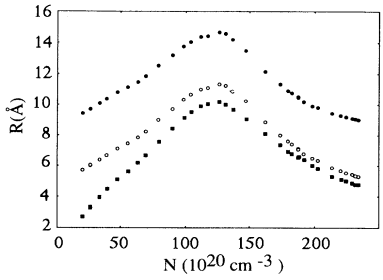

FIG. 8. Semihydrodynamic radius of the ion as a function of the gas density. Closed squares: pure Stokes calculated from Eq. (21); closed circles: Stokes-Cunningham calculated from Eq. (26); open circles: modified Stokes-Cunningham calculated from Eq. (29). It has to be noted that Eq. (21) and Eq. (29) give a radius that at high density tends to the value 4.36 Å of one solvation shell of neon atoms tightly packed around the ion.

by Atkins [56] for ions in liquid helium. This model, which treats the fluid as a continuum, is based on the fact that when a polarizable fluid is distributed throughout a nonuniform electric field, its density and pressure increase with increasing field. An ion in the gas produces a very strong electric field in its proximity and the mean gas density steadily increases as the ion is approached. Moreover, since the gas viscosity is an increasing function of density, electrostriction produces an increase of the viscous drag that would be normally exerted on a neutral body of the same size of the ion. The hydrodynamic problem to be solved is the determination of the drag force on a spherical particle of radius R and velocity $v_D = \mu E$, which acts on the surrounding gas so as to maintain a given radial density and viscosity variation $N(r)$ and $\eta(r)$. This goal has been accomplished by Ostermeier and Schwarz [57] (OS) who solved the Navier-Stokes equations, supplemented with the continuity equation of the fluid, allowing for a spatial dependence of density and viscosity. The result for the mobility can be expressed in terms of a Stokes-like formula as

$$\mu = \frac{e}{6\pi\eta_\infty RF} \tag{30}$$

where η_∞ is the viscosity of the unperturbed fluid. F is a correction term which depends on the gas through η_∞ and N_∞ (the density of the unperturbed fluid), as well as on the charge-fluid interaction through the shape of the density and viscosity disturbances. According to OS, F can be calculated by solving the following equation:

$$y^2 f''' + \left[2y - 2y^2\frac{\rho'}{\rho} + y^2\frac{\eta'}{\eta}\right] f'' + \left[-6 + 2y^2\left(\frac{\rho'}{\rho}\right)^2 - y^2\frac{\rho''}{\rho} - y^2\frac{\rho'\eta'}{\rho\eta}\right] f'$$

$$+ \left[6\frac{\rho'}{\rho} - 4y\left(\frac{\rho'}{\rho}\right)^2 + 2y\frac{\rho''}{\rho} + 2y\frac{\rho'\eta'}{\rho\eta}\right] f - \frac{9\rho F}{\eta} = 0 \tag{31}$$

where $y = R/r$ is the inverse of the distance from the ion center in units of the bare ion radius. Primes indicate differentiation with respect to y and F is expressed in units of $6\pi\eta_\infty R v_D$. $f(y)$ is the function describing the velocity profile of the gas in the forward direction in front of the moving particle and is subjected to the usual boundary conditions that the fluid velocity at the ion equals the ion velocity (no-slip condition) and that the fluid at large distance is at rest. The correction term F can be computed by Taylor-expanding f around $y = 1$ and substituting it into Eq. (31). If there are m terms in the series expansion of f, one gets a set of $m+1$ linear algebraic equations for the coefficients of the expansion and for F, which can be solved with usual matrix inversion methods [41].

In order to solve Eq. (31) we need to calculate the density and viscosity profiles as determined by electrostriction. According to Atkins [56], the gas is treated as a classical continuum whose relative dielectric constant $K(N)$ is related to the gas density by the usual Clausius-Mossotti formula

$$\frac{K-1}{K+2} = \frac{N\alpha}{3\epsilon_0} \tag{32}$$

where the atomic polarizability α and N are expressed in mks units.

This classical approximation should be fairly good, except in close proximity of the ion. Nonetheless, as pointed out by OS, the most important effects are those due to density and viscosity disturbances which extend farther out from the ion into the fluid. Assuming that the system is in thermodynamic equilibrium, the chemical potential of the gas atoms must be uniform throughout the whole system. Therefore, if $g_0(T,P)$ is the chemical potential of the gas atoms in the unperturbed region, in the region where the electric field generated by the ion is $\mathbf{E}_i$ the chemical potential must be modified so as to yield

$$g(r) = g_0 - \frac{1}{2}\frac{\mathbf{P}\cdot\mathbf{E}_i}{N} \tag{33}$$

where $\mathbf{P}$ is the polarization of the medium [58]. Since g and T are constant throughout the fluid ($dg = 0$, $dT = 0$), differentiation of Eq. (33) yields

$$\frac{dP}{N} = \frac{1}{N}\left(\frac{\partial P}{\partial N}\right)_T dN = \frac{\mathbf{P}\cdot d\mathbf{E_i}}{N} \tag{34}$$

where P is the fluid pressure. Upon integration we get

$$\int_{N_\infty}^{N(r)} \frac{1}{N}\left(\frac{\partial P}{\partial N}\right)_T dN = \tfrac{1}{2}\alpha {E_i}^2(r) \tag{35}$$

where $E_i(r)$ is the electric field of the ion at a distance r. (Strictly speaking, we should use here the local field at the atom, but the factor $3/[2+K(N)]$ is practically equal to 1 even at the highest density.) By substituting in Eq. (35) for $E_i(r)$ its actual expression $E_i(r) = -e/[4\pi\epsilon_0 K(N) r^2]$ and collecting all density-dependent terms we obtain

$$\mathcal{G}(N,N_\infty) = [K(N)]^2 \int_{N_\infty}^{N} \frac{1}{N}\left(\frac{\partial P}{\partial N}\right)_T dN = \frac{1}{2}\frac{\alpha e^2}{(4\pi\epsilon_0)^2 r^4}. \tag{36}$$

The left-hand side of Eq. (36) can be easily evaluated as a function of N and N_∞ since the equation of state of neon is known [43] and the density profile is then determined by inverting Eq. (36) to yield

$$r = \left[\frac{1}{2}\frac{\alpha e^2}{(4\pi\epsilon_0)^2 \mathcal{G}(N,N_\infty)}\right]^{1/4}. \tag{37}$$

In Fig. 9 we report some of the density profiles obtained and in Fig. 10 the corresponding viscosity profiles computed by exploiting the known density dependence of η. We must point out, however, that the uncertainty in the viscosity is quite large since there are no measurements at precisely the same temperature and density of our experiment and we had to interpolate and extrapolate available literature data [50].

The effect of electrostriction is to enhance the local density around the ion. For densities of the unperturbed gas lower than the critical one, there is a spatial region where the local density passes through the critical value and the corresponding profile is very steep as a consequence of the large compressibility of the gas. The density profiles become less and less steep as the unperturbed gas density increases, and, eventually, for densities of the unperturbed gas larger than the critical one the density profiles are very gentle, since the gas compressibility is no longer as large as before.

From Fig. 9 we can also note that for small distances all profiles converge to a single curve. This means that close to the ion the local density is fairly independent of the mean gas density. Moreover, we observe that the spatial extent of the density disturbance increases with increasing the unperturbed gas density up to the critical value, when it reaches its maximum value because of the large gas compressibility. Then, for larger gas densities the spatial extent of the density profiles decreases.

These density and viscosity profiles can be now in-

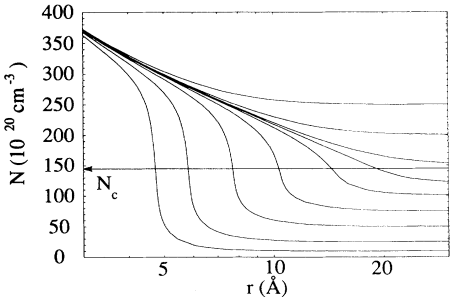

FIG. 9. Profiles of the local density around the ion calculated according to the Atkins electrostriction model. The densities of the unperturbed gas are (from bottom to top) $N = (10, 25, 50, 75, 100, 120, 150, 200, 250) \times 10^{20}$ cm^{-3}.

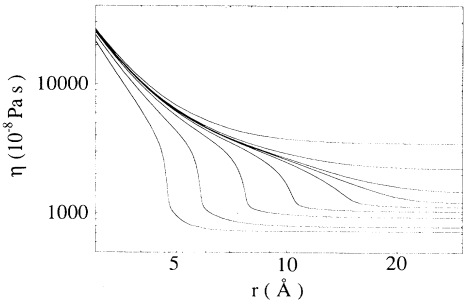

FIG. 10. Profiles of the local viscosity around the ion calculated according to the Atkins electrostriction model. The densities of the unperturbed gas are (from bottom to top) $N = (10, 25, 50, 75, 100, 120, 150, 200, 250) \times 10^{20}$ cm^{-3}.

serted into Eq. (31) and the correction factor F can be calculated. We have to point out that the density profiles calculated as previously described do not allow for the short-range repulsive part of the ion-atom interaction. To take this into account, the profiles are cut off at a given hard-sphere radius of the bare ion so that $N(r \leq R) = 0$. As a result, the correction factor F depends on the choice of this value.

In Fig. 11 we show the F values calculated for some values of the bare ion hard-sphere radius R. For all R F has the same general behavior showing a maximum at a density close to, but smaller than the critical one in agreement with the semihydrodynamic radius calculated from the experimental data. The correction factor F decreases with increasing cutoff radius, as is to be expected since for large distances the local density tends towards the unperturbed one, thus canceling out the effects of electrostriction. We have to point out that the calculations were not performed for densities lower than those shown in Fig. 11 because the steepness of the relative density profiles was so large as to give numerical problems when solving Eq. (31).

Finally, in Fig. 12 we compare the experimental $\mu_0 N$

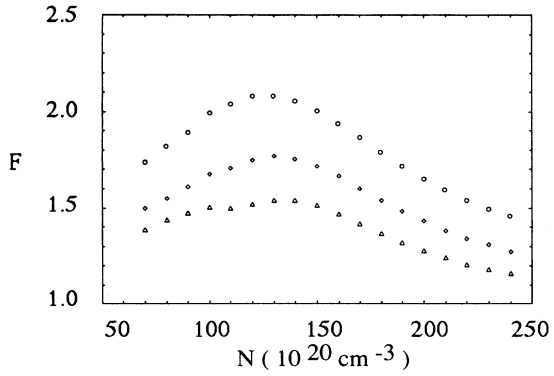

FIG. 11. Density dependence of the correction factor F calculated according to the Ostermeier-Schwarz model by solving the Navier-Stokes equation with spatially dependent density and viscosity. The cutoff hard-sphere radii are (from top to bottom) $R = (3.2, 4.0, 5.0)$ Å, respectively.

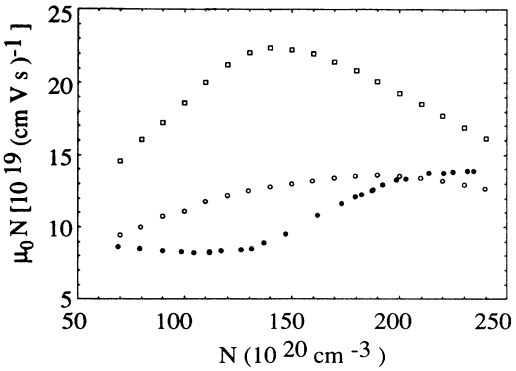

FIG. 12. Zero-field density-normalized ion mobility as a function of the gas density. Closed circles: experimental data; open circles: prediction of the OS theory with a hard-sphere cutoff radius $R = 4$ Å; open squares: prediction of the pure Stokes' formula with the same R.

data with the prediction of the electrostriction theory Eq. (30) as well as with the prediction of the pure Stokes formula which neglects electrostriction, Eq. (21). The results obtained by neglecting electrostriction differ largely from the experimental data. On the contrary, the results obtained by using electrostriction are in better agreement with the experiment showing deviations within 40%.

We believe that the residual discrepancies might be attributed to several reasons. Density profiles as steep as those reported in Fig. 9 for densities lower than the critical one are not very realistic and are not compatible with the assumption of local thermodynamic equilibrium. It is also questionable if the continuum approximation can be adopted at a distance from the ion comparable with the atomic diameter, especially when density is so rapidly varying. From Fig. 12 we see that the largest discrepancy among theory and experiment occurs around the critical density and below it. At lower densities the mean free path of the ion is relatively bigger than at larger densities and the ion passes through the gas without a fully developed density profile. The effective density profile should be then obtained by averaging the calculated profiles over a mean free path, thus yielding a less steep but farther extending density disturbance which results in a larger F factor. On the other side of the density range the ion mean free path is much smaller than one atomic diameter and the effective density profile should be very close to the computed ones. The agreement between theory and experiment in this region is better, indeed. The idea of averaging over a distance of the order of the ion mean free path is supported also by the following arguments. The buildup of the density profiles in response to the disturbance produced in the gas by the ion can fully develop only if the ion velocity is smaller than the sound velocity in the gas, in order that the fluid can react readily to the presence of the moving ion. The ion velocity to be considered is the thermal one

$$\bar{v} = \left(\frac{8k_B T}{\pi M_e}\right)^{1/2} \tag{38}$$

where M_e is the effective ion mass. According to [47], approximately ten atoms are tightly bound to the ion so that $M_e \simeq M_{O_2} + 10M_{Ne}$. This yields $\bar{v} \simeq 64$ m/s. The sound velocity in neon, c, can be estimated from the equation of state by means of the usual formula

$$c = \left(\frac{N_A \gamma}{M_{Ne} N \chi_T} \right)^{1/2} \tag{39}$$

where N_A is Avogadro's number, $\gamma \simeq \frac{5}{3}$, and χ_T is the isothermal compressibility [59]. We get $c \simeq 154$ m/s for $N = 15 \times 10^{20}\,\mathrm{cm}^{-3}$, $c \simeq 19$ m/s for $N = 150 \times 10^{20}\,\mathrm{cm}^{-3}$, and $c \simeq 85$ m/s for $N = 240 \times 10^{20}\,\mathrm{cm}^{-3}$. We see that the sound velocity is always comparable with the ionic thermal velocity and close to the critical density it is even smaller than that. Thus the gas has no time to react instantaneously to the passage of the charge.

Finally, we want to recall here briefly the existence of a theory for the ionic mobility in liquids, proposed by Davis, Rice, and Meyer [60] as an extension of the Rice-Allnatt theory [61] for transport processes in simple liquids to the mobility case. This theory is essentially based on the knowledge of the ion–neutral-atom pair correlation function and has been successfully exploited to calculate the mobility of positive ions in liquid Ar, Kr, and Xe [60,62]. The Atkins electrostriction model was used to calculate the long-range part of the pair correlation function as

$$g_p(r) = \frac{N(r) - N_\infty}{N_\infty}. \tag{40}$$

This is just what we have done in this work. The drawback of this theory, however, is the lack of knowledge of the short-range part of the correlation function of the ion–neutral-species system, which was either calculated numerically for a Lennard-Jones fluid modeling the actual system, or was assumed to be equal to the pair correlation function of the solvent. On the contrary, in the OS scheme all quantities are, in principle, known, and using this approach we have been able to numerically reproduce the mobility of positive ions in liquid Ar, Kr, and Xe without any adjustable parameter [63].

[1] E.A. Mason and E.W. McDaniel, *Transport Properties of Ions in Gases* (Wiley, New York, 1988).
[2] E.W. McDaniel and E.A. Mason, *The Mobility and Diffusion of Ions in Gases* (Wiley, New York, 1973).
[3] G.R. Freeman and D.A. Armstrong, in *Advances in Atomic and Molecular Physics*, edited by D. Bates and B. Bederson (Academic, New York, 1985), Vol. 20, p. 267.
[4] B.L. Henson, Phys. Rev. Lett. **24**, 1327 (1970); Phys. Rev. **135**, 1002 (1964).
[5] S. Cunsolo and P. Mazzoldi, Nuovo Cimento **20**, 949 (1961).
[6] G. Careri, U. Fasoli, and F.S. Gaeta, Nuovo Cimento **15**, 774 (1960).
[7] B. Brody, Phys. Rev. B **11**, 170 (1975).
[8] L. Meyer and F. Reif, Phys. Rev. **110**, 279 (1958).
[9] F. Reif and L. Meyer, Phys. Rev. **119**, 1164 (1960).
[10] W.I. Glaberson and W.W. Johnson, J. Low Temp. Phys. **20**, 313 (1975).
[11] B.E. Springett, Phys. Rev. **184**, 229 (1969).
[12] L. Bruschi, P. Mazzoldi, and M. Santini, Phys. Rev. **167**, 203 (1968).
[13] F. Scaramuzzi, A. Savoia, D.L. Goodstein, and M.W. Cole, J. Phys. C **10**, L413 (1977).
[14] I. Modena and F.P. Ricci, Phys. Lett. **25A**, 213 (1967).
[15] M.W. Cole and R.A. Bachman, Phys. Rev. **B 15**, 1388 (1977).
[16] D.L. Goodstein, J. Low Temp. Phys. **33**, 137 (1978).
[17] M.W. Cole and F. Toigo, Phys. Rev. B **17**, 2054 (1978).
[18] R.M. Bowley, J. Phys. C **11**, 75 (1978); J. Low Temp. Phys. **24**, 41 (1976).
[19] T.H. Dey and T.J. Lewis, Brit. J. Appl. Phys. **1**, 1019 (1968).
[20] N. Gee, M. Antonio Floriano, T. Wada, S.S.-S. Huang, and G.R. Freeman, J. Appl. Phys. **57**, 1097 (1985).
[21] N. Gee and G.R. Freeman, Can. J. Chem., **58**, 1490 (1980).
[22] S.S.-S. Huang and G.R. Freeman, J. Chem. Phys. **72**, 1989 (1980).
[23] N. Gee, S. S.-S. Huang, T. Wada, and G.R. Freeman, J. Chem. Phys. **77**, 1411 (1982).
[24] N. Gee and G.R. Freeman, Can. J. Chem. **59**, 2988 (1981).
[25] R.E. Voshall, J.L. Pack, and A.V. Phelps, J. Chem. Phys. **43**, 1990 (1965).
[26] L. Bruschi, M. Santini, and G. Torzo, J. Phys. B **17**, 1137 (1984).
[27] A.F. Borghesani and M. Santini, in *Gaseous Dielectrics VI*, edited by L.G. Christophorou and I. Sauers (Plenum, New York, 1991), p. 27.
[28] A.K. Bartels, Phys. Lett. **45A**, 491 (1973).
[29] L.G. Christophorou, D.L. McCorkle, and A.A. Christodoulides, in *Electron-Molecule Interactions and Their Applications*, edited by L.G. Christophorou (Academic, Orlando, 1984).
[30] A.K. Bartels, Ph.D. thesis, University of Hamburg (1971) (unpublished).
[31] G.H. Wannier, *Statistical Physics* (Dover, New York, 1966).
[32] E. Vogt and G.H. Wannier, Phys. Rev. **95**, 1190 (1954).
[33] J.A. Jahnke, M. Silver, and J.P. Hernandez, Phys. Rev. **B 12**, 3420 (1975).
[34] A.F. Borghesani, L. Bruschi, M. Santini, and G. Torzo, Rev. Sci. Instrum. **57**, 2234 (1986).
[35] A.F. Borghesani, L. Bruschi, M. Santini, and G. Torzo, Phys. Rev. **A 37**, 4828 (1988).
[36] A.F. Borghesani and M. Santini, Phys. Rev. A **42**, 7377 (1990).
[37] A.F. Borghesani, L. Bruschi, M. Santini, and G. Torzo, Z. Naturforsch. **41a**, 912 (1986).
[38] A.F. Borghesani and G. Delfitto, Meas. Sci. Technol. **1**, 825 (1990).
[39] A.F. Borghesani and M. Santini, Meas. Sci. Technol. **1**, 939 (1990)
[40] B.A. Younglove, J. Phys. Chem. Ref. Data, **11** (1982)

(Appendix K).
[41] W.H. Press, B.P. Flannery, S.A. Teukolski, and W.T. Vetterling, *Numerical Recipes. The Art of Scientific Computing* (Cambridge University Press, Cambridge, 1986).
[42] D. Neri, Tesi di Laurea, University of Padua (1991) (unpublished).
[43] R.D. McCarty and R.B. Stewart, Natl. Bur. of Stand. (U.S.) Misc. Publ. No. 8726 (U.S. GPO, Washington, D.C., 1965).
[44] G.C. Maitland, M. Rigby, E.B. Smith, and W.A. Wakeham, *Intermolecular Forces. Their Origin and Determination* (Oxford University Press, Oxford, 1981).
[45] C. Kittel, *Introduction to Solid State Physics* (Wiley, New York, 1986).
[46] J.O. Hirschfelder, C.F. Curtiss, and R.B. Bird, *Molecular Theory of Gases and Liquids*, (Wiley, New York, 1954).
[47] E.L. Pollock and B.J. Alder, Phys. Rev. Lett. **41**, 903 (1978).
[48] R.B. Bird, W.E. Stewart, and E.N. Lightfoot, *Transport Phenomena* (Wiley, New York, 1960).
[49] B.J. Alder and E. Alley, Phys. Today **37** (1), 56 (1984).
[50] V.A. Rabinovitch, V.I. Nedostup, A.A. Vasserman, and L.S. Veksler, in *Thermophysical Properties of Neon, Argon, Krypton, and Xenon*, National Standard Reference-Data Service of the U.S.S.R. (Hemisphere, Washington, D.C., 1988).
[51] F. Reif, *Fundamentals of Statistical and Thermal Physics* (McGraw-Hill, Singapore, 1965).
[52] E. Cunningham, Proc. R. Soc. London Ser. A **83**, 357 (1910).
[53] A.M. Tyndall, *The Mobility of Positive Ions in Gases* (Cambridge University Press, Cambridge, 1938).
[54] J.L. Levine and T.M. Sanders, Phys. Rev. **154**, 138 (1967).
[55] Yu.A. Berlin, L. Nyikos, and R. Schiller, J. Chem. Phys. **69**, 2401 (1978).
[56] K.R. Atkins, Phys. Rev. **116**, 1339 (1959).
[57] R.M. Ostermeier and K.W. Schwarz, Phys. Rev. A **5**, 2510 (1972).
[58] E.A. Guggenheim, *Thermodynamics* (North-Holland Amsterdam, 1967).
[59] M.W. Zemanski and R.H. Dittman, *Heat and Thermodynamics* (McGraw-Hill International Editions, Singapore, 1987).
[60] H.T. Davis, S.A. Rice, and L. Meyer, J. Chem. Phys. **37**, 2470 (1962).
[61] S.A. Rice and A.R. Allnatt, J. Chem. Phys. **34**, 2144 (1961).
[62] L. Palleschi, S. Sacchetta, and F.P. Ricci, Mol. Phys. **42**, 961 (1981).
[63] D. Neri (private communication).